IJME

Int. J. of Applied Mechanics and Engineering, 2026, vol.31, No.1, pp.165-185
DOI: 10.59441/ijame/218162

EFFECT OF CHEMICAL REACTION ON HEAT AND MASS TRANSFER OF POROUS MHD CASSON NANO FLUID WITH MELTING AND JOULE HEATING

Namala Yuvaraju [1*] and D. Hymavathi [2]
[1]Department of Mathematics, Sreenidhi Institute of Science and Technology,
Hyderabad, Telangana, INDIA
[2]Department of Mathematics, University College of Science,
Mahatma Gandhi University, Nalgonda, Telangana, INDIA
E-mail: yuvaraju.n@sreenidhi.edu.in

The purpose of this study is to use computational tools to evaluate the effects of Joule heating, chemical reactions and melting on heat and mass transfer of a non-Newtonian Casson nano fluid flow across a porous stretched surface. The governing equations containing partial derivatives are consistent with nonlinear ordinary differential equations. The transformations are subject to the similarity variable, which is employed in the equation's solution. To generate approximate answers, a numerical method based on the Shoot technique and the Runge-Kutta method is used. A graphic representation of the velocity, temperature, and concentration distributions is shown. Additionally defined for specific parameter values are skin friction, Nusselt number, and Sherwood number. According to the study's key findings, boosting the Joule heating parameter enhances the temperature profiles, increasing Magnetic and Permeability parameters decreases velocity but increases temperature. Porous material is found to have a considerable effect on the problem's flow and thermal properties. When the current analysis findings are compared to the existing literature in specific settings, better agreement is observed.

Key words: Casson nano fluid, chemical reaction, melting, Joule heating, stretching surface.

1. Introduction

The Newtonian fluids model is unable to account for every flow characteristic seen in modern technology. As a result, the notion of non-Newtonian fluid flow has gained significance. These investigations have several applications, including casting, paper manufacture, and polymer extrusion. Casson fluid is one of these non-Newtonian liquids that has caught the attention of many researchers because of its potential in drilling techniques, bioengineering procedures, and other fields. Human blood, tomato sauce, and jelly are some of the main Casson fluids. Magnetohydrodynamics (MHD) is modern building science that involves magnetic field interaction with electrically conductive fluids. Casson [1] first used the Casson fluid flow model to forecast how well pigment-oil suspensions would work. Casson fluid is among the most utilized viscoelastic non-Newtonian materials. Casson liquid colloidal reactions involved both heterogeneous and homogeneous chemical species. A numerical data analysis indicated that the Casson term modified flow behavior by enhancing viscosity. The fluid material's yield stress does not generate flow and thus has zero viscosity at infinite nonlinear shear rates [2]. Pramanik [3] explored the Casson fluid flow and radiation effects on stretched surfaces in porous media. El-Aziz and Afify [4] examined the unsteady MHD flow of Casson liquid across a stretched plate, considering numerous characteristics. Eldabe and Salwa [5] studied Casson fluid flow in spinning cylinders.

There are many peer-to-peer uses for the mechanism of heat transmission and flow via stretched surfaces. These include making fiberglass, making paint and lubricants work better, molding plastic, blowing glass, making paper, growing crystals, and many others. The heat transfer rate determines the final product's

* To whom correspondence should be addressed

features. Kishan and Shashidar [6] investigated the effect of heat flux on a non-Newtonian fluid passing through a porous moving surface while accounting for viscous dissipation.

The conversion of raw materials into finished goods is dependent on chemical reactions in many industrial processes. These processes are vital to produce fertilizers, agricultural inputs, fuels, polymers, and pharmaceuticals. Additionally, chemical reactions have a vital function in the food sector, where they improve flavour and preservation, generate energy through combustion, and tackle environmental challenges through waste treatment and pollution control. Sadiq *et al.* [7] provided the precise answers for mass and heat transfer in second-grade nanofluids characterized by chemical reactions, wall sliding, and heat generating. The Yanala *et al.* [8] examined three-dimensional radiative MHD Casson fluid flow across an extended permeable surface with a chemical reaction. Anwar *et al.* [9] investigated MHD convection at a stagnation point in a non-Newtonian fluid characterized by yield stress and chemical processes.

Thermal radiation-based heat transfer is widely used in various technical operations, including gas turbines, satellites and spacecraft, nuclear power plants, missiles, and the thrust mechanism for aviation engines. The effects of heat transport and radiation on the Williamson reactive fluid were discussed individually in previous studies [10, 11]. Makinde [12] studied free convection and radiation on a vertical porous surface. Das [13] discussed how radiation and slippage affect MHD flow on a flat plate. Mukhtar *et al.* [14] computed heat transfer in a flow of Maxwell nanofluid subjected to magnetohydrodynamics (MHD) via a stretched flat surface, accounting for radiation.

Researchers have made substantial progress in solving the melting heat transfer problem because of its many industrial and technological uses, such as solidifying molten rock flows, thawing frozen ground, and preparing semiconductor substances. Yacob *et al.* [15] investigated micropolar fluid for melting heat transfer at the stagnation point across stretching/shrinking surfaces, whereas Bachok *et al.* [16] investigated steady flow across moving surfaces for melting heat transmission. Mabood and Das [17] showed how second-order slip and melting heat transfer with radiation affect MHD nanofluid flow. Fazle and Kalidas [18] examined how melting affects the MHD flow of Casson fluid across a stretching surface. Alsulami and Hymavathi [19] investigates how 2D micropolar nanofluid flow across a permeable stretchable surface with a stagnation point is affected by Brownian motion, thermophoresis, internal heat generation/absorption, chemical reactions, and melting effects.

Joule heating impacts the entire electrical conductor, whereas the Peltier effect primarily influences the transmission of heat between electrical junctions. Joule heating, also known as resistive heating, is employed in a wide range of electrical and industrial applications. The heating element transforms heat from electrical energy. Another name for Joule heating is resistive heating, which is used in various industrial and technological applications. The heating element is the component that converts power to heat. When grid electricity is available, electric heaters are commonly used to heat buildings. Joule heating is used to cook food in electric stoves and ovens. Electrical components can be linked by melting conductive solder using the heat of a soldering iron. Cartridge heaters are utilized in numerous manufacturing processes. Electric fuses melt when exposed to a current greater than their melting point as a safety measure. Ehsan *et al.* [20] investigated the effects of Joule heating on heat transfer and entropy generation in MHD channel flow using a parametric investigation and a PINN-based solution to an ill-posed issue. Yuvaraju *et al.* [21] discusses the combined effects of velocity slip and Joule heating in MHD Casson-Williamson nanofluids that move through a stretching porous material. Ahmad *et al.* [22] examined how slips and Joule heating impact MNF flow on a narrow surface. Numerous authors, such as [23, 24], have explored nanofluid research.

This study examines the efficiency of chemical reactions in relation to the movement of nanoparticles induced by Joule heating and melting within a Casson non-Newtonian nanofluid. Previous research has revealed that there are few papers in the literature that discuss mass transfer's impact on MHD Casson nanofluid flows. Shashidar Reddy *et al.* [26] examined how chemical reaction and melting affect the MHD flow of Casson fluid across a stretching surface without Joule heating. Hence, our principal goal is to fill such a void. Extending the work of Shashidar Reddy [26] is the focus of this study. This study is unique in investigating the effectiveness of chemical reactions in a Casson non-Newtonian nanofluid as nanoparticles move due to Joule heating. And it investigates how Casson nanofluid flow across a porous stretched surface is impacted by thermophoresis, Brownian motion, internal heat, mass generation/absorption, and melting effects. The flow's governing equations are solved numerically, and the effects of key factors are visually examined.

2. Formulation of model

A mathematical representation of 2D continuous flow of an MHD Casson nanofluid past a stretching sheet is shown in Figure 1. This presupposes that the sheet is straight and horizontal, that there is a porous medium, and that the fluid gradually melts into a constant property. The preferred Cartesian model limits flow to $y > 0$ and aligns the *x*-axis with the surface and the *y*-axis perpendicular to the sheet. An application of a magnetic field in the normal direction is designed to cause fluid to conduct electricity. Assuming $c > 0$ and $a > 0$, let $u_w(x) = cx$ represent the stretched sheet velocity and $u_e(x) = ax$ represent the external flow velocity. Melting and Liberation T_m and T_∞ are the liquid stream temperatures, respectively.
The following are the constituent equations that determine the Casson liquid:

$$\tau_{ij} = \begin{cases} 2\left(\mu_B + \dfrac{P_y}{\sqrt{2\pi}}\right)e_{ij}, & \pi > \pi_c \\ 2\left(\mu_B + \dfrac{P_y}{\sqrt{2\pi_c}}\right)e_{ij}, & \pi < \pi_c \end{cases} \tag{2.1}$$

where P_y is fluid yield stress, μ_B is plastic dynamic viscosity, $\pi = e_{ij}e_{ij}$ is deformation rate, π_c is product's non-Newtonian critical value, and e_{ij} is deformation rate's $(i, j)^{th}$ component.
The fluid exhibits solid-like behaviour when the shear stress is below the yield stress and commences movement when the shear stress exceeds the yield stress.

Joule heating occurs as a result of an electric field within the fluid. Assumptions may encompass constant electrical conductivity, uniform distribution of the electric field, and the exclusion of magnetic field influences on electrical conductivity (if relevant).
The equations governing the flow under the conditions are [26]:

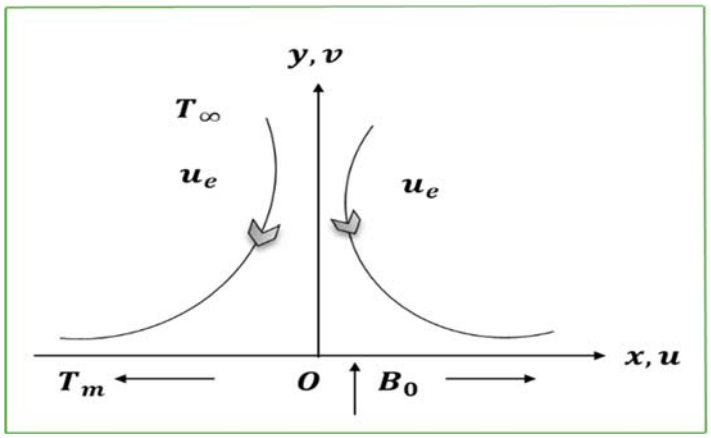

Fig.1. Coordinate system and physical model.

$$\frac{\partial u}{\partial x} + \frac{\partial v}{\partial y} = 0, \tag{2.2}$$

$$u\frac{\partial u}{\partial x} + v\frac{\partial u}{\partial y} = u_e\frac{du_e}{dx} + \nu\left(1 + \frac{1}{\beta}\right)\frac{\partial^2 u}{\partial y^2} - \frac{\sigma B_0^2}{\rho}(u - u_e) - \frac{\nu}{K}(u - u_e), \tag{2.3}$$

$$u\frac{\partial T}{\partial x}+v\frac{\partial T}{\partial y}=\alpha\frac{\partial^2 T}{\partial y^2}-\frac{1}{\rho C_P}\frac{\partial q_r}{\partial y}+\tau\left[D_B\frac{\partial C}{\partial y}\frac{\partial T}{\partial y}+\frac{D_T}{T_\infty}\left(\frac{\partial T}{\partial y}\right)^2\right]+\frac{\sigma B_0^2}{\rho C_p}u^2, \tag{2.4}$$

$$u\frac{\partial C}{\partial x}+v\frac{\partial C}{\partial y}=D_B\frac{\partial^2 C}{\partial y^2}+\frac{D_T}{T_\infty}\frac{\partial^2 T}{\partial y^2}-kr\left(C-C_\infty\right). \tag{2.5}$$

Subject to the limit conditions,

$$\begin{aligned} &u=u_w(x)=cx,\quad T=T_m,\quad C=C_w \quad \text{at} \quad y=0,\\ &u\to u_e(x)=ax,\quad T\to T_\infty,\quad C\to C_\infty \quad \text{as} \quad y\to\infty \end{aligned} \tag{2.6}$$

and $$k\left(\frac{\partial T}{\partial y}\right)_{y=0}=\rho\left[\lambda+c_s\left(T_\infty-T_0\right)\right]v(x,0). \tag{2.7}$$

Here, β is Casson nano fluid parameter, α is thermal diffusivity, k is thermal conductivity, K is permeability , u and v are components of velocity, λ is latent heat, ρ is the density the fluid, ν is kinematic viscosity, q_r is radiative heat flux, c_s is heat capacity, c_p is specific heat at constant pressure, k_1 is rate of reaction and D_B is mass diffusion.

Using Rosseland's estimate [25], we have

$$q_r=-\frac{16\sigma^*}{3k^*}T_\infty^3\frac{\partial T}{\partial y}. \tag{2.8}$$

Where σ^* is Stefan-Boltzmann's constant and k^* is the absorption's coefficient respectively
Eq.(2.4), can be written using Eq.(2.8) as

$$u\frac{\partial T}{\partial x}+v\frac{\partial T}{\partial y}=\alpha\frac{\partial^2 T}{\partial y^2}+\frac{1}{\rho C_P}\frac{16\sigma^*}{3k^*}T_\infty^3\frac{\partial^2 T}{\partial y^2}+\tau\left[D_B\frac{\partial C}{\partial y}\frac{\partial T}{\partial y}+\frac{D_T}{T_\infty}\left(\frac{\partial T}{\partial y}\right)^2\right]+\frac{\sigma B_0^2}{\rho C_p}u^2. \tag{2.9}$$

Here are the relations that have been introduced:

$$u=\frac{\partial\psi}{\partial y},v=-\frac{\partial\psi}{\partial x},\psi=x\sqrt{a\nu}f(\eta),\eta=\sqrt{\frac{a}{\nu}}y,\theta=\frac{T-T_m}{T_\infty-T_m},\phi=\frac{C-C_\infty}{C_w-C_\infty}. \tag{2.10}$$

Where ψ is referred to as the flow's stream function.
By substituting the above considerations (2.10) in the governing Eqs (2.3), (2.9), (2.5) and boundary conditions can be obtained a

$$\left(1+\frac{1}{\beta}\right)f'''+ff''-f'^2+(M+P)(1-f')+1=0, \tag{2.11}$$

$$(1+R)\theta'' + Prf\theta' + PrNt\theta'^2 + PrNb\theta'\phi' + PrJf'^2 = 0\,, \tag{2.12}$$

$$\phi'' + Scf\phi' + \frac{Nt}{Nb}\theta'' - ScA\phi = 0\,. \tag{2.13}$$

Subject to the requirements for the boundaries:

$$\begin{aligned} &f'(\eta) = \varepsilon, \quad Prf(\eta) + Me\theta'(\eta) = 0, \quad \theta(\eta) = 0, \quad \phi(\eta) = 0 \quad \text{at} \quad \eta = 0, \\ &f'(\eta) = 0, \quad \theta(\eta) = 1, \quad \phi(\eta) = 1 \quad \text{as} \quad \eta \to \infty. \end{aligned} \tag{2.14}$$

Where $\beta = \mu_B \frac{\sqrt{2\pi_c}}{P_y}$, $M = \frac{\sigma B_0^2}{\rho a}$, $P = \frac{\nu}{Ka}$, $R = \frac{16\sigma^*}{3kk^*}T_\infty^3$, $k = \alpha\rho c_p$, $\varepsilon = \frac{c}{a}$, $Pr = \frac{\nu}{\alpha}$,

$Me = \frac{c_p(T_\infty - T_m)}{\lambda + c_s(T_m - T_0)}$ $Nt = \frac{\tau D_T(T_\infty - T_m)}{T_\infty \nu}$, $Nb = \frac{\tau D_B(C_w - C_\infty)}{\nu}$, $J = \frac{ax^2\sigma B_0^2}{\rho c_p(T_\infty - T_m)}$,

$Sc = \frac{\nu}{D_B}$, $A = \frac{kr}{a}$.

Physical amounts like Skin friction quantifies the shear stress exerted by the fluid flowing over a surface due to viscous forces, Sherwood number deals with transfer of mass and is the ratio of convective to diffusive mass transfer and for a given length, and Nusselt number is the ratio of the convective to conductive heat transfer. They can be stated as follows:

$$Re_x^{\frac{1}{2}} C_f = \left(1 + \frac{1}{\beta}\right) f''(0)\,, \quad \frac{Nu_x}{Re_x^{\frac{1}{2}}} = -(1+R)\theta'(0)\,, \quad \frac{Sh_x}{Re_x^{\frac{1}{2}}} = -\phi'(0). \tag{2.15}$$

Where $Re_x = \frac{xu_e}{\nu}$ is the local Reynolds number.

3. Method of solution

We solved the ordinary differential Eqs (2.11) through (2.13) along with the associated boundary and initial conditions (2.14) using the most efficient numerical approach, which was based on the R-K method technique. The numerical solutions are produced using MATLAB's symbolic programming.
Let

$$f = y_1, \quad f' = y_1' = y_2, \quad f'' = y_2' = y_3, \quad f''' = y_3',$$

$$\theta = y_4, \quad \theta' = y_4' = y_5, \quad \theta'' = y_5',$$
$$\phi = y_6, \quad \phi' = y_6' = y_7, \quad \phi'' = y_7',$$

$$=> y_1' = y_2, \quad y_1(0) = -\frac{Me}{Pr} y_5, \quad y_2(0) = \varepsilon = \frac{c}{a},$$

$$y_4(0) = 0, \quad y_6(0) = 0.$$

After considering the above specified parameters, we arrived at the following results.

$$f''' = y_3' = \left(\frac{\beta}{1+\beta}\right)\left[(y_2)^2 - y_1 y_3 + (M+P)(y_2 - 1) - 1\right], \tag{3.1}$$

$$\theta'' = y_5' = \left(\frac{1}{1+R}\right)\left[-Pry_1 y_5 - PrNt(y_5)^2 - PrNby_5 y_7 - PrJ(y_2)^2\right], \tag{3.2}$$

$$\begin{aligned}\phi'' = y_7' = ScAy_6 - Scy_1 y_7 - \frac{Nt}{Nb} y_5' = ScAy_6 - Scy_1 y_7 + \\ + \frac{Nt}{(1+R)Nb}\left[Pry_1 y_5 + PrNt(y_5)^2 + PrNby_5 y_7 + PrJ(y_2)^2\right].\end{aligned} \tag{3.3}$$

You can use the fourth-order RK approach to integrate the previously specified seven simultaneous equations and conditions of first order. The technique is continued until the results reach the anticipated accuracy level of 10^{-7} to fulfil the convergence criterion.
Shooting technique uses the Runge-Kutta method to transform boundary value problems into initial value problems. This is commonly used in fluid mechanics, Engineering and Physics such as for solving non-linear differential equations that require specific values at both ends of a range.

3.1. Procedure of Runge-Kutta method

- Define the ordinary differential equation function: create a MATLAB function that represents the right-side of ODE
- Initialize parameters: Define the initial conditions, step size, and the range over which you want to solve the ODE.
- Implement the RK4 algorithm: use a loop to iterate through the independent variable values and apply the RK4 formulas to calculate the corresponding dependent variable values.
- Visualize the results: Plot the numerical solution to see how independent variable changes with independent variable.

4. Results and discussion

The impact of several parameters Me, β, Pr, P, R, M, Sc, Nt, Nb, J, A, including $\varepsilon = 0.5$ or 1.5, on velocity, temperature, and concentration fields that determine fluid flow behavior is studied numerically in order to gain a thorough comprehension of the problem's physical model.

Figure 2 Shows how velocity profiles vary Stretching parameter (ε), Magnetic parameter (M) and Porosity parameter (P). Fig.2(a) clearly shows that as M grows, the flow rate and velocity drop. The Lorentz force slows the velocity of conducting fluid in the boundary layer, which accounts for this. As seen in Fig.2(b), P has the same influence. It is important to note that all these outcomes occur when $\varepsilon = 1.5$, whereas the effect is opposite when $\varepsilon = 0.5$.

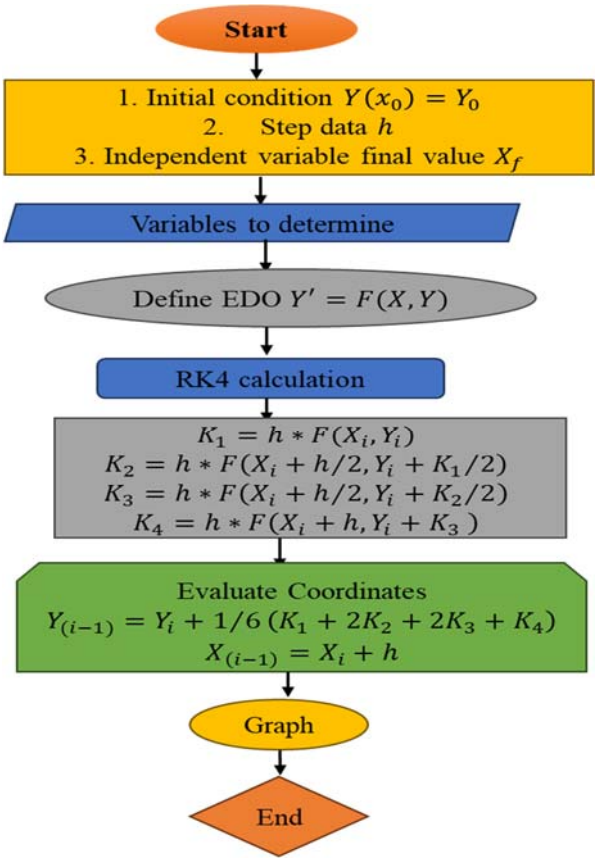

Fig.2. Flow chart of the Runge-Kutta method.

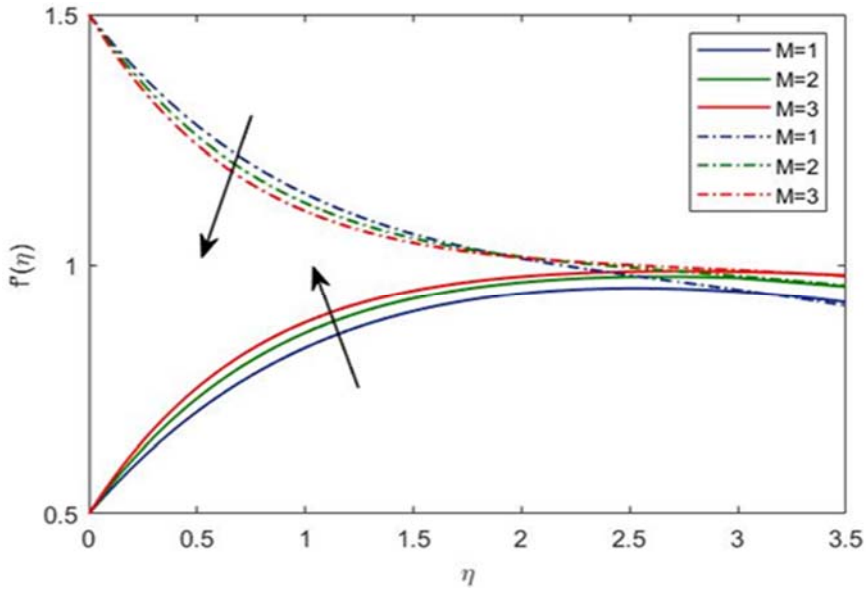

Fig.2(a). M and ε v/s velocity.

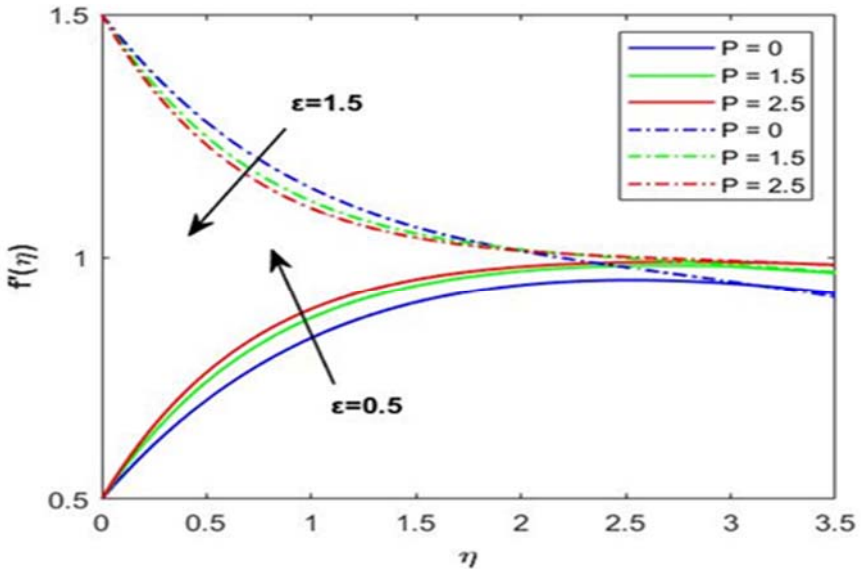

Fig.2(b). P and ε v/s velocity.

The effect of the β and Pr examining the velocity profiles of both $\varepsilon = 1.5$ and $\varepsilon = 0.5$ is shown in Fig.3(a) and 3(b). The graphs clearly show that when $\varepsilon = 1.5$, fluid motion decreases with β. This is because of a higher β value results in a lower yields stress and a more viscous fluid. As a result, the fluid's motion slows. However, when $\varepsilon = 0.5$, the results are inverted. The fluid completely acts like a Newtonian fluid for varying values of β. when compared to Newtonian fluids, the Casson fluid has a thicker velocity boundary layer as a result. However, for both circumstances of $\varepsilon = 1.5$ and 0.5, fluid motion rises as the Prandtl number grows.

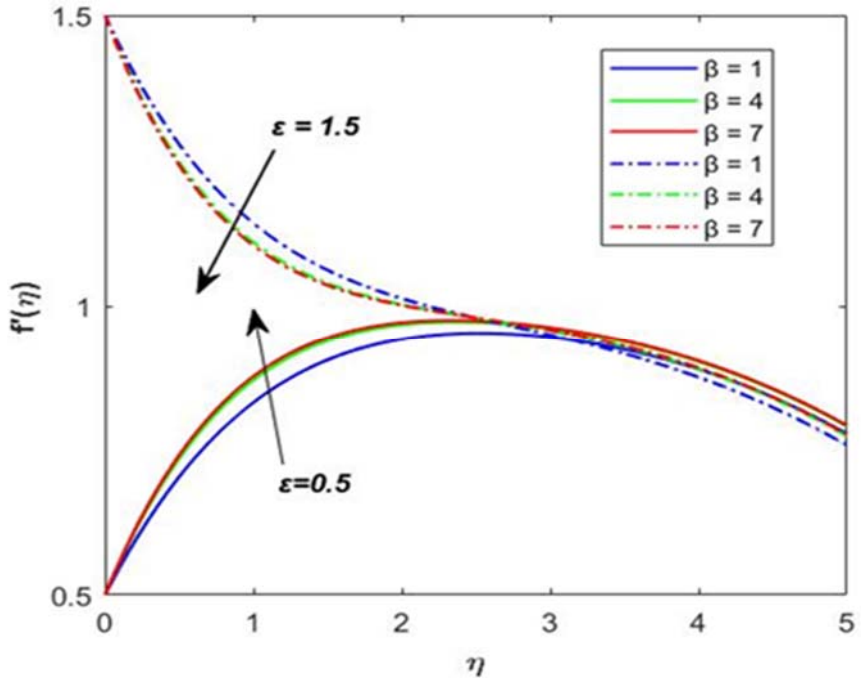

Fig.3(a). β and ε v/s velocity.

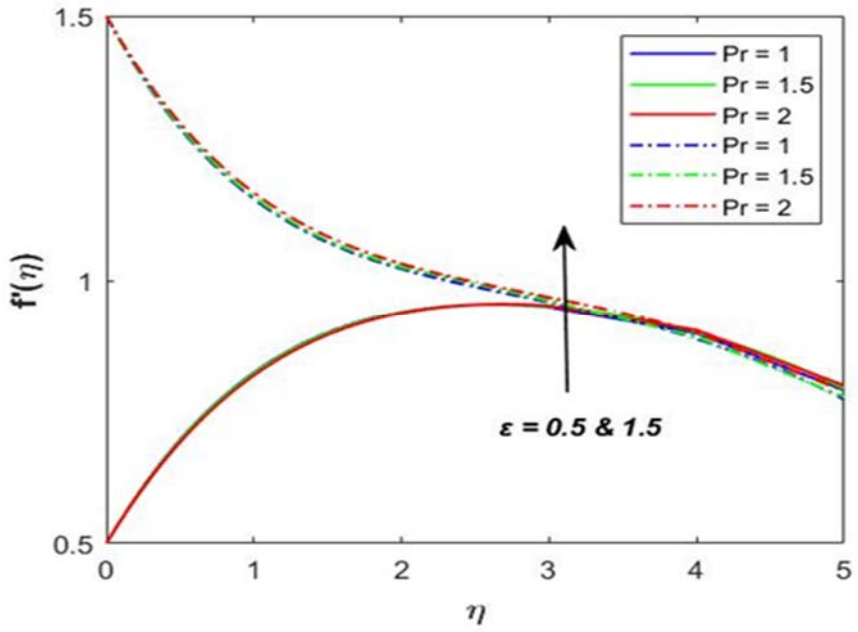

Fig.3(b). Pr and ε v/s velocity.

Figure 4(a) and 4(b) depicts temperature curves for different M and P values, while other parameters remain constant. The figures clearly illustrate that, for $\varepsilon = 0.5$ and $\varepsilon = 1.5$ circumstances, the temperature of fluid increases when the magnetic and porosity parameters increase. The Lorentz force raises the fluid temperature, which supports this claim.

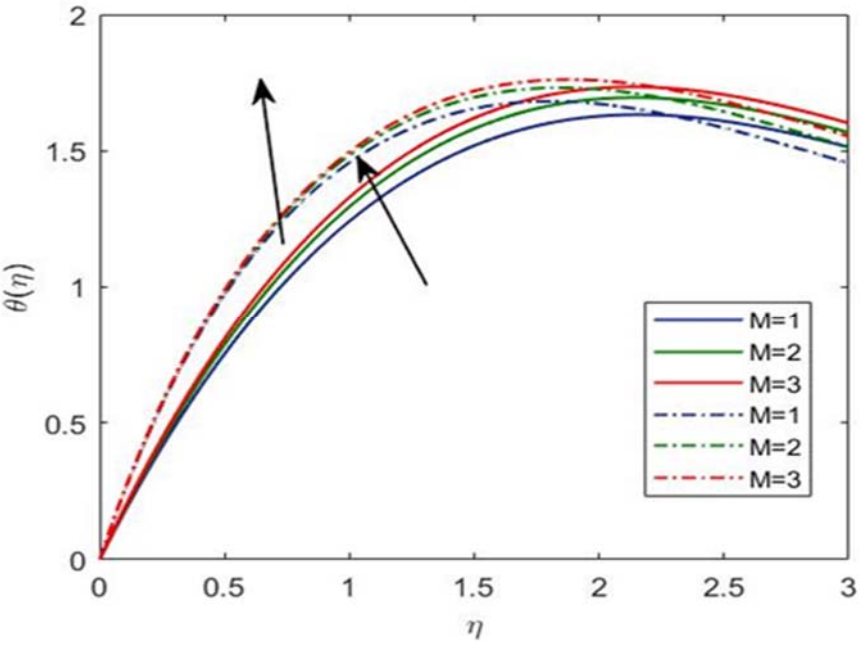

Fig.4(a). M and ε v/s temperature.

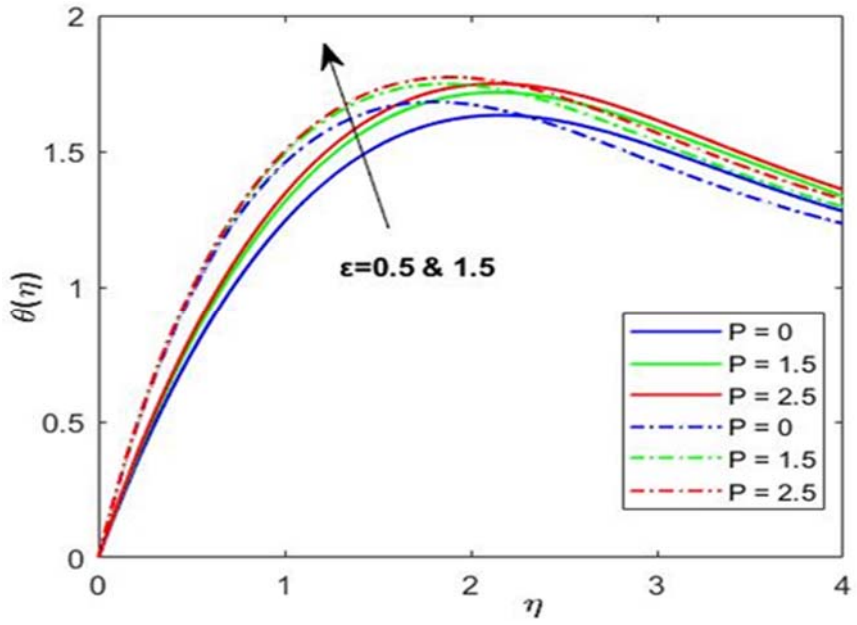

Fig.4(b). P and ε v/s temperature.

Figure 5(a) depicts the magnetic field's effect on Casson fluid parameter β on temperature. It is worth noting that as β grows (for $\varepsilon = 0.5$ and $\varepsilon = 1.5$), the thermal boundary layer becomes slightly thicker. Casson fluids have a yield stress, which means they will not flow until the shear force that is applied is larger than the yield stress. The fluid starts to flow and the Casson plastic viscosity goes up a lot as the shear rate goes up. Higher shear rates can make viscosity less obvious and make things act more like liquids. However, as illustrated in Fig.5(b), the fluid temperature rises significantly as Pr increases. The Pr represents the ratio of momentum to thermal diffusivities. A higher Prandtl value indicates lower thermal diffusivity. A small amount of heat transfer from the heated fluid to the melting surface keeps the temperature high.

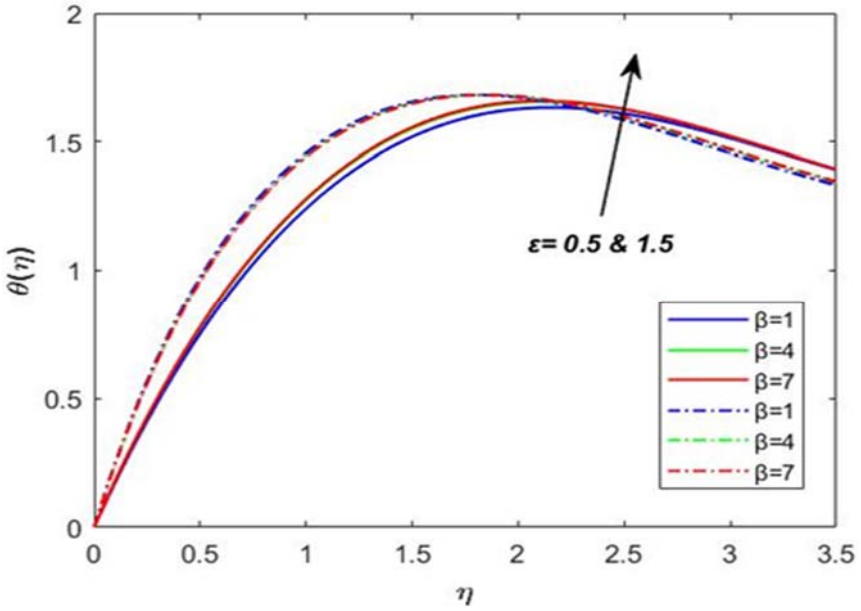

Fig.5(a). β and ε v/s temperature.

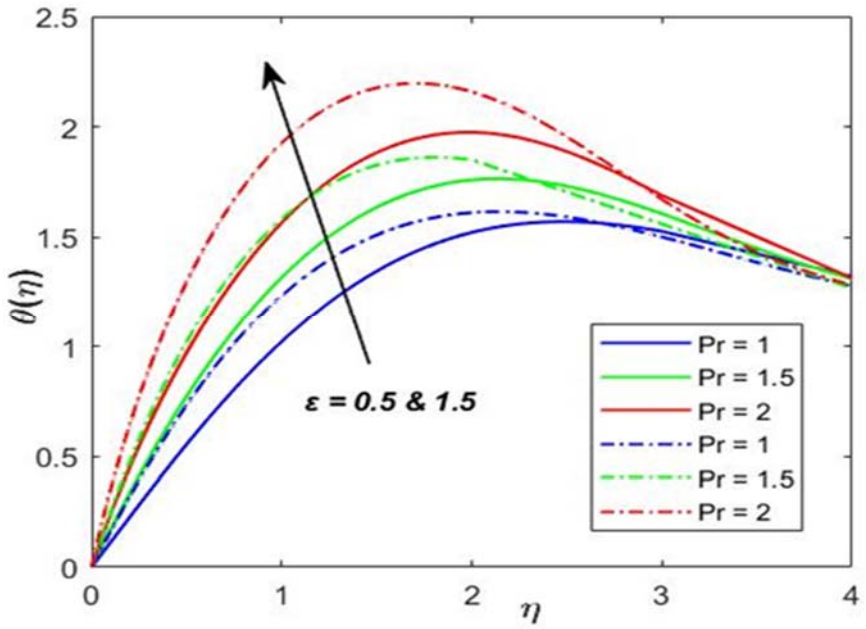

Fig.5(b). Pr and ε v/s temperature.

Figure 6 is examined, impact of the R and Me on fluid temperature for $\varepsilon = 0.5$ or 1.5. As the R rises, the temperature falls, as seen in Fig.6(a). This is because radiation accelerates the rate at which heat flows over a melting surface. Furthermore, Fig.6(b) shows how the melting parameter Me influences temperature. Between T_m at the surface and T_∞ at infinity, the temperature of Casson nano fluid levels steadily decline. The temperature at the boundary layer decreases in both cases of stretching parameter scenarios.

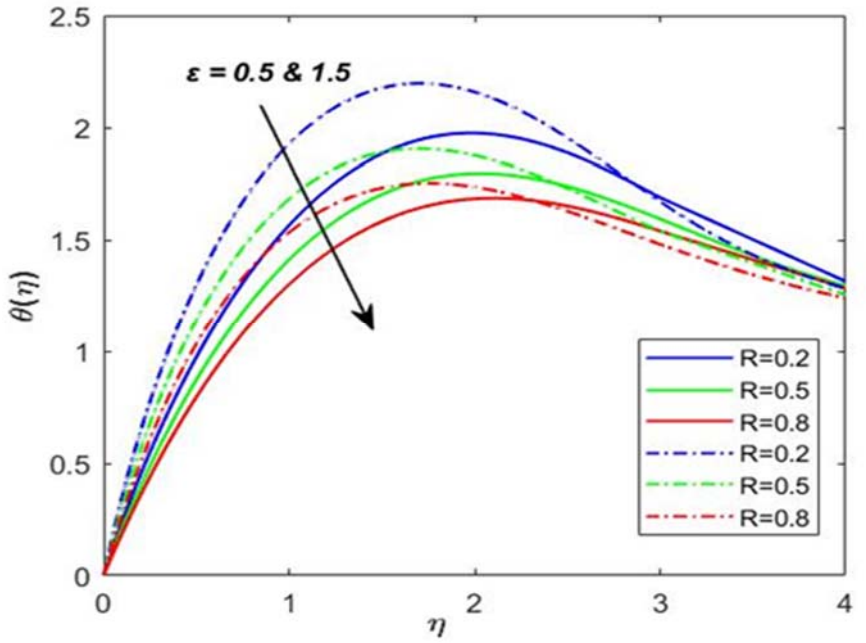

Fig.6(a). R and ε v/s temperature.

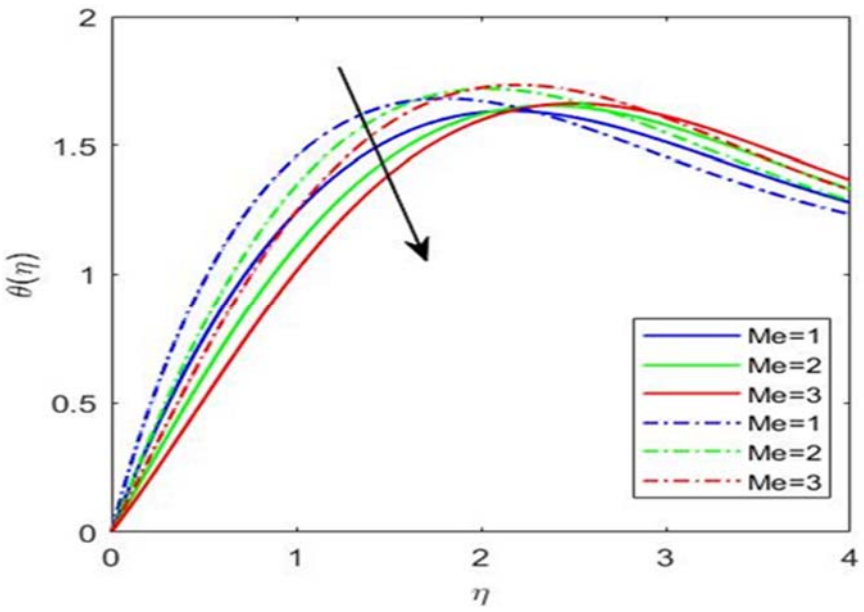

Fig.6(b). *Me* and ε *v* / *s* temperature.

Figure 7 illustrates how the Schmidth number *Sc* and chemical reaction *A* affect concentration profiles for $\varepsilon = 0.5$ or *1.5*. According to the graph Fig.7(a), the concentration profile increases as *Sc* increase. Figure 7(b) shows the concentration profiles as the chemical reaction parameter *A* changes. The graph clearly shows that a drop in the concentration field corresponds to an increase in the chemical process.

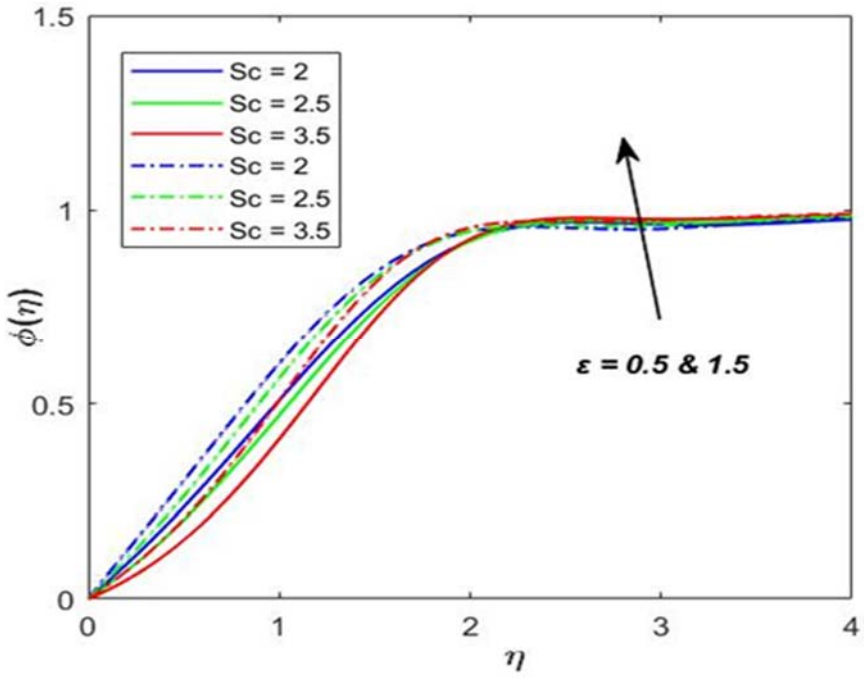

Fig.7(a). *Sc* and ε *v* / *s* concentration.

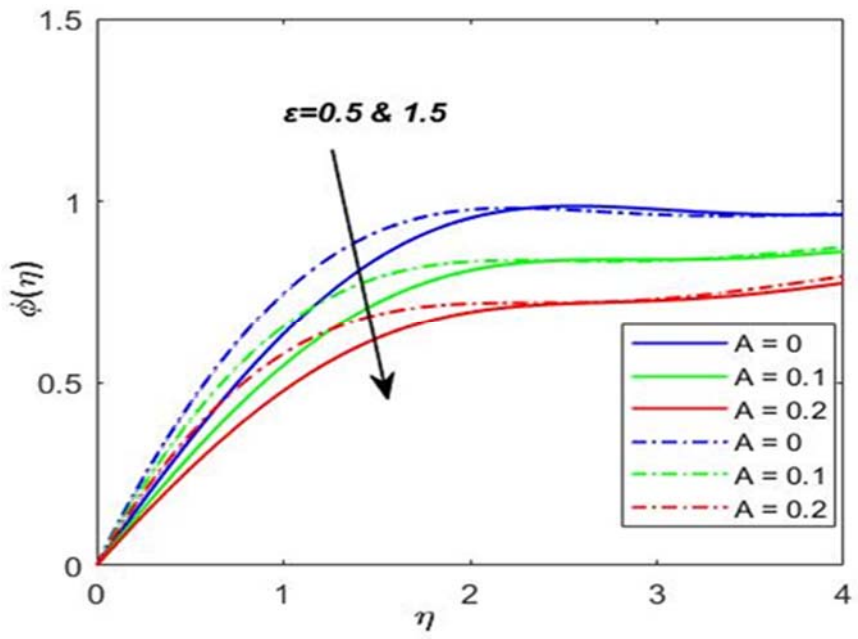

Fig.7(b). A and ε v/s concentration.

Figure 8 depicts varying values of the thermophoresis factor Nt for the temperature circulation of the thermal boundary layer for $\varepsilon = 0.5$ or 1.5. Thermophoresis is a force of transport caused by temperature gradients. As Nt increases, the boundary layer becomes denser, elevating the surface temperature and signalling an increase in temperature at $\varepsilon = 0.5$ and 1.5.

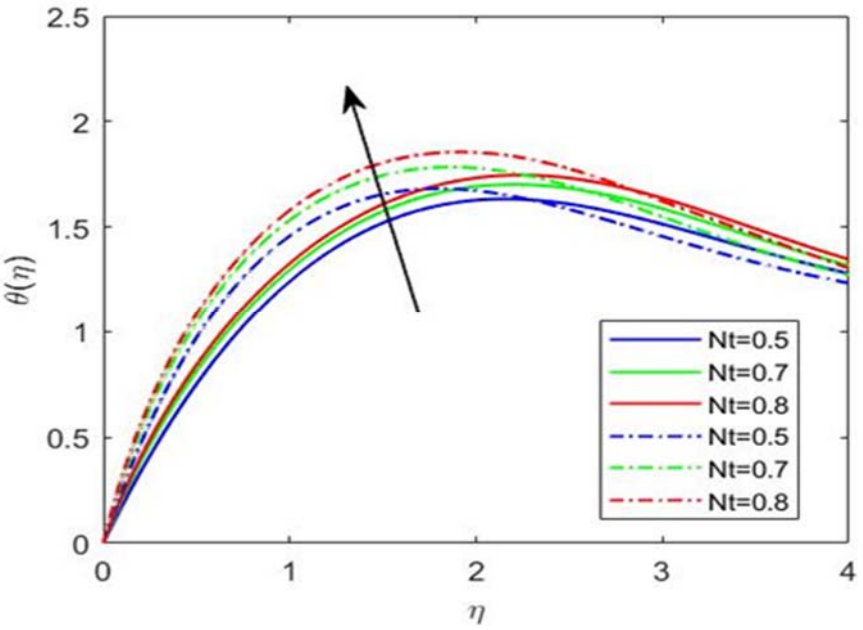

Fig.8. Nt and ε v/s temperature.

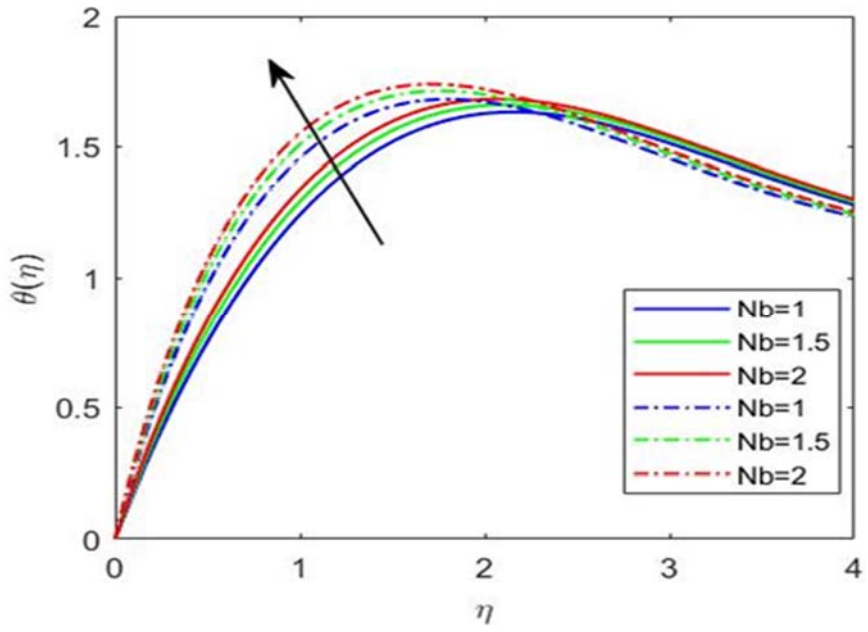

Fig.9. *Nb* and ε *v / s* temperature.

Figure 9 shows the thermal boundary layer temperature dispersion for a few Brownian motion *Nb* simulations for $\varepsilon = 0.5$ or *1.5*. Brownian motion is the motion caused by numerous collisions of molecules in a fluid. This volatile motion accelerates the collisions between fluid molecules and nanoparticles. In both cases $\varepsilon = 0.5$ and *1.5*, the temperature increases when molecules transform their kinetic energy into thermal energy.

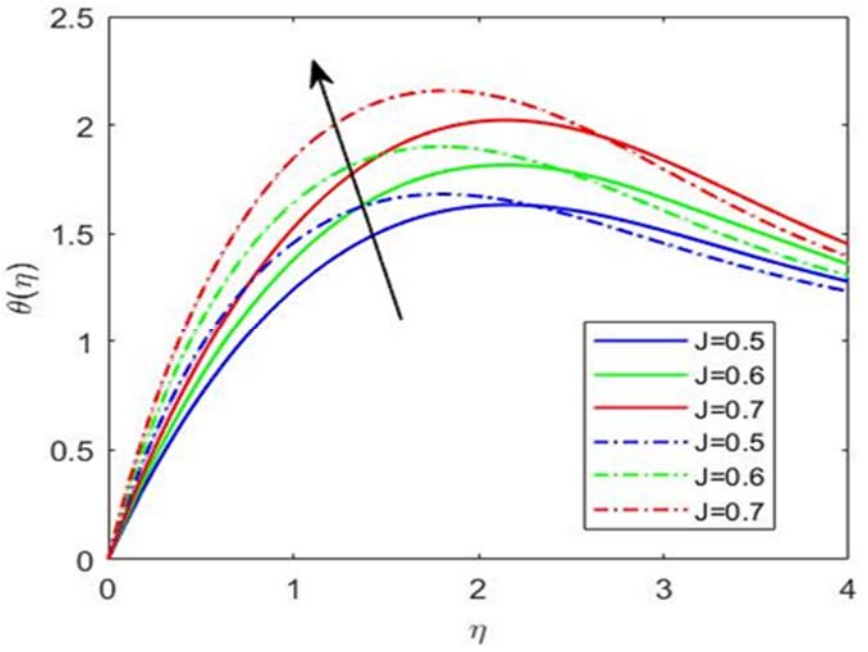

Fig.10. *J* and ε *v / s* temperature.

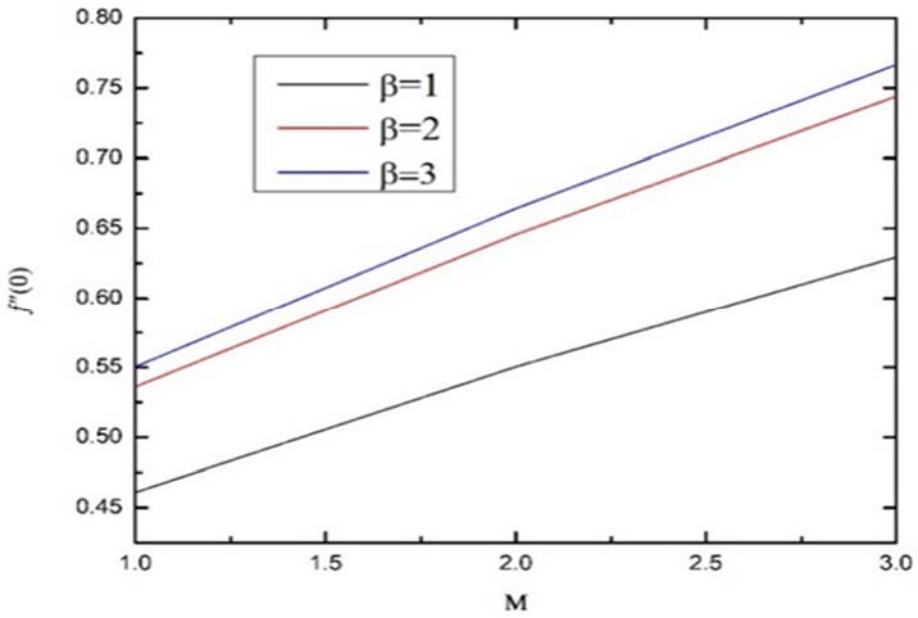

Fig.11. M and v/s $f''(0)$.

In MHD nanofluid systems, current flows through the conductive fluid, resulting in Joule heating. As illustrated in Fig.10, the Joule heating process in an MHD nanofluid causes the temperature to rise. This is due to the nanoparticles increased electrical conductivity being directly proportional to the increase in heat output for a given amount of current. Joule heating generates heat, raising the fluid's temperature at $\varepsilon = 0.5$ and 1.5.

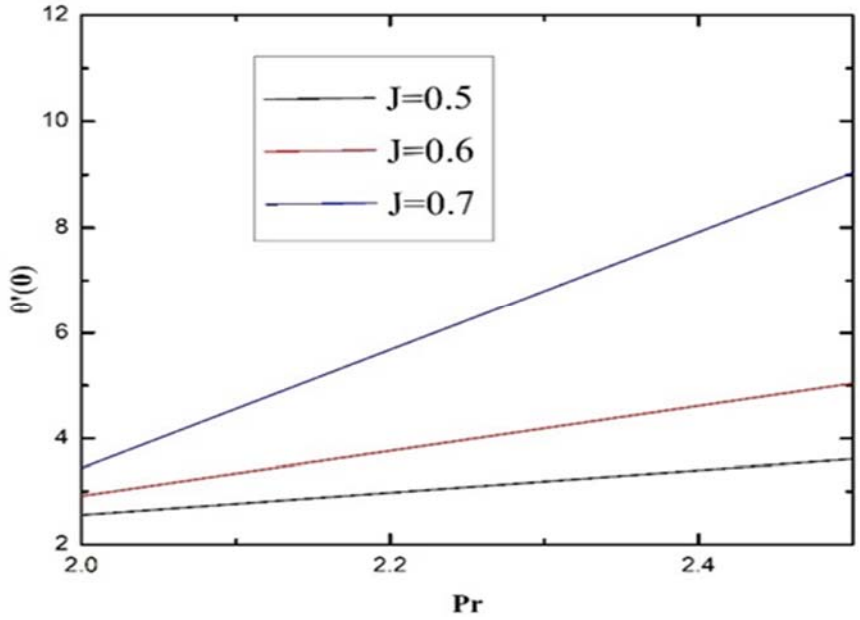

Fig.12. Pr and v/s $\theta'(0)$.

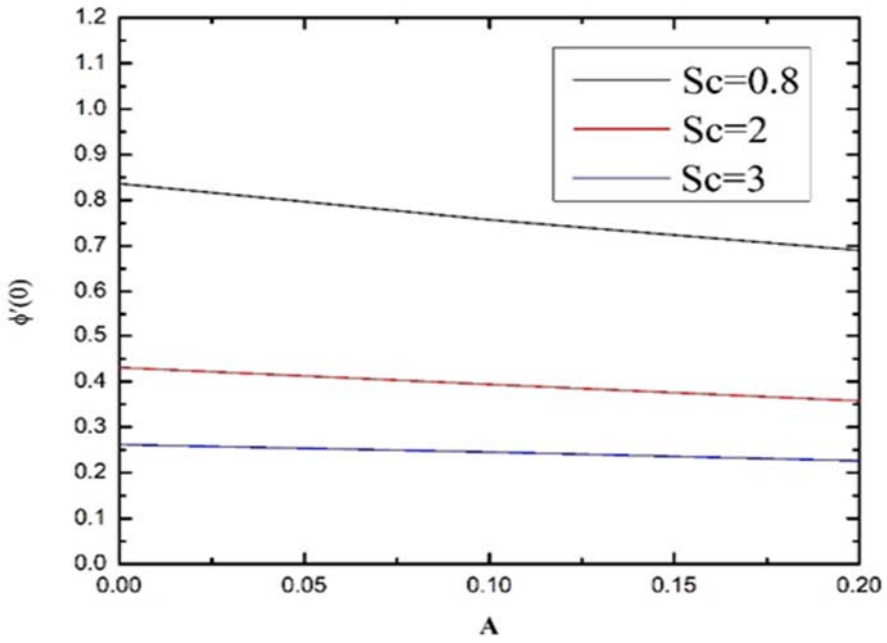

Fig.13. A and v/s $\phi'(0)$.

Figure 11explains skin friction values rise in parallel with increases in Casson nano fluid and magnetic field parameters. As Prandtl number and Joule heating parameters are grow, the heat transfer rate (Nusselt number) increases, as shown in Fig.12. It has been discovered that the mass transfer rate (Sherwood number) decreases with increasing chemical reaction and Schmidth number values, as shown in Fig.13.

Table 1 displays intriguing data on skin friction, Nusselt number, and Sherwood number for various parameters. The numerical values of the mass transfer coefficient, heat rate, and skin friction rate for various M, P, β, ε, Pr, R, Me, Sc, A, Nt, Nb and J values are displayed in Tab.1. The tabulated data show that skin friction coefficient, Sherwood, and Nusselt numbers are increases when Casson nano fluid parameter increase. In addition, as the Joule heating parameter rises, $f''(0)$ decreases, but $\theta'(0)$, and $\phi'(0)$ are increases.

Table 2 shows that for given stretching parameter values, the melting and stretching parameters reduce skin friction. Table 3 indicates that Nusselt number increases with stretching values but reduces with melting parameter. A comparative analysis is conducted by tabulating the current results alongside the previous data [22] to validate the numerical method. The values are found to be in very good agreement. In addition, the Sherwood number is calculated for various A and ε values in Tab.4 to investigate the effect of chemical reactions on liquid concentration. The table clearly shows that the Sherwood number drops as A increases, but increases with stretching values.

Table 1. For dissimilar approximations for dimensionless variables, the numerical $f''(0)$, $\theta'(0)$ and $\phi'(0)$ approximations are shown as follows.

M	***P***	***β***	***Pr***	***R***	***Me***	***Sc***	***A***	***Nt***	***Nb***	***J***	$f''(0)$	$\theta'(0)$	$\phi'(0)$
1											*0.460826*	*2.559681*	*0.836526*
2											*0.550428*	*2.676929*	*0.850651*
3											*0.629633*	*2.755618*	*0.860968*
	0										*0.460826*	*2.559681*	*0.836526*
	1.5										*0.591078*	*2.719639*	*0.856144*

Table 1 cont. For dissimilar approximations for dimensionless variables, the numerical $f''(0), \theta'(0)$ and $\phi'(0)$ approximations are shown as follows.

M	***P***	***β***	***Pr***	***R***	***Me***	***Sc***	***A***	***Nt***	***Nb***	***J***	$f''(0)$	$\theta'(0)$	$\phi'(0)$
	2.5										*0.666357*	*2.787519*	*0.865286*
		1									*0.460826*	*2.559681*	*0.836526*
		4									*0.536089*	*2.646314*	*0.850864*
		7									*0.550332*	*2.660752*	*0.853367*
			2								*0.460826*	*2.559681*	*0.836526*
			2.5								*0.444587*	*3.613520*	*1.187690*
			3								*0.396900*	*5.907919*	*1.736168*
				0.2							*0.460826*	*2.559681*	*0.836526*
				0.5							*0.478535*	*2.211661*	*0.787927*
				0.8							*0.491874*	*1.957524*	*0.750918*
					1						*0.460826*	*2.559681*	*0.836526*
					2						*0.440722*	*1.485737*	*0.299572*
					3						*0.430123*	*1.065528*	*0.105604*
						0.8					*0.460826*	*2.559681*	*0.836526*
						2					*0.469135*	*2.394815*	*0.430671*
						3					*0.473172*	*2.315727*	*0.261494*
							0				*0.460826*	*2.559681*	*0.836526*
							0.1				*0.467711*	*2.422847*	*0.757507*
							0.2				*0.473075*	*2.317600*	*0.690239*
								0.5			*0.460826*	*2.559681*	*0.836526*
								0.7			*0.415837*	*3.509429*	*1.404544*
								0.8			*0.364062*	*4.695790*	*1.900236*
									1		*0.460826*	*2.559681*	*0.836526*
									1.5		*0.452995*	*2.717846*	*0.620734*
									2		*0.446859*	*2.843742*	*0.504821*
										0.5	*0.460826*	*2.559681*	*0.836526*
										0.6	*0.443288*	*2.917823*	*0.847588*
										0.7	*0.419044*	*3.438063*	*0.849047*

Table 2. Comparison of $f''(0)$ when $Pr = 1,\ Sc = 0.1,\ A = M = P = R = J = 0,\ \beta \to \infty$ for various values of ε and Me.

	results of Shashidar Reddy [26]			**present results**		
ε	***Me*** $= 0$	***Me*** $= 1$	***Me*** $= 2$	***Me*** $= 0$	***Me*** $= 1$	***Me*** $= 2$
0	*1.248743*	*1.038628*	*0.943157*	*1.245571*	*1.019456*	*0.935672*
0.5	*0.729753*	*0.605187*	*0.548776*	*0.712471*	*0.599247*	*0.526894*
1	*0*	*0*	*0*	*-0.028028*	*-0.009201*	*-0.005324*
2	*-1.980601*	*-1.626101*	*-1.468287*	*-1.924856*	*-1.563230*	*-1.395082*

Table 3. Comparison of $\theta'(0)$ when $Pr = 1,\ Sc = 0.1,\ A = M = P = R = J = 0$, $\beta \to \infty$ for various values of ε and Me.

	results of Shashidar Reddy [26]		**present results**	
ε	$Me = 0$	$Me = 1$	$Me = 0$	$Me = 1$
0	0.559217	0.364089	0.575682	0.412864
0.5	0.671162	0.4414	0.682645	0.483942
2	0.92051	0.620226	1.056382	0.666429
5	1.247393	0.870098	1.304283	0.909437

Table 4. Comparison of $\phi'(0)$ when $Pr = 1,\ Sc = 0.1, M = P = R = 0, Me = J = 0$, $\beta \to \infty$ for various values of ε and A.

	results of Shashidar Reddy [26]		**present results**	
ε	$A = 0$	$A = 1$	$A = 0$	$A = 1$
0	0.271286	0.202069	0.665436	0.431742
0.5	0.285227	0.212885	0.791523	0.537919
2	0.316475	0.2372	1.087210	0.793863
5	0.358346	0.269971	1.514314	1.173580

5. Conclusion

Numerical analysis is utilized to investigate the evolution of heat and mass transmission in Casson nanofluid flow across a porous melting stretched surface under joule heating and chemical reactions. Using the shooting approach and the Runge-Kutta method, the modified flow equations are numerically solved. A graphic illustration of the effect of many significant parameters on the velocity, temperature, and concentration fields is shown.

The following is a list of notable finds:

- The Casson nano fluid parameter, porosity, Prandtl number, and magnetic parameter all contribute to a drop in velocity, which reduces the thickness of the velocity boundary layer.
- Porosity, Prandtl number, and magnetic field all raise the fluid's temperature.
- Temperature of the fluid enhances with the Casson fluid parameter and hence thickening the temperature boundary layer.
- Thermal radiation and melting actions cause temperature distribution to degrade.
- The temperature profiles change as the Brownian motion parameter increases. The chaotic movement of particles in fluids brought on by frequent of molecular collisions is known as Brownian motion. Volatile motion accelerates collisions between fluid and nanoparticles. Temperature increases when molecules transform their kinetic energy into thermal energy.
- The Schmidt number helps to increase the liquid's concentration. Concentration is reduced by enhancing chemical reaction parameter.
- Skin friction is reduced by the melting and stretching factors.
- The solid-fluid interface’s local Nusselt number falls as melting and radiation rise, whereas the converse is true for the Casson nano fluid parameter.
- Joule heating produces heat by raising the temperature of the fluid.

Acknowledgments

The authors express appreciation to the reviewers and editor for their valuable suggestions, which enhanced the quality of this work. The authors express gratitude to the management of SNIST and MG University for providing the necessary facilities to conduct the research.

Nomenclature

A – chemical reaction parameter
c_s – heat capacity $\left(kg / ms^2\right)$
c_p – the specific heat at constant pressure $\left(kg / ms^2\right)$
D_B – mass diffusion
J – Joule heating parameter
K – permeability
k – thermal conductivity $\left(W \cdot m^{-1} \cdot K^{-1}\right)$
k_1 – rate of reaction
M – magnetic parameter
Me – melting parameter
Nb – Brownian motion
Nt – thermophoresis
P – porosity factor
Pr – Prandtl number
q_r – radiative heat flux $\left(W / m^2\right)$
R – radiation parameter
Sc – Schmidt number
u, v – velocity components $\left(m / s\right)$
x, y – axis coordinates $\left(m\right)$

Greek symbols

α – thermal diffusivity $\left(m^2 / s\right)$
β – Casson nano fluid parameter
ε – stretching parameter
λ – latent heat
ν – kinematic viscosity $\left(m^2 / s\right)$
ρ – fluid's density $\left(kg / m^3\right)$

abbreviations

MHD – magnetohydrodynamics
MNF – Maxwell nanofluid

References

[1] Casson N. (1959): *A flow equation for the pigment oil suspensions of the printing ink type.*– Mills C.C. (Ed.), Rheology of Disperse Systems. Pergamon Press, Oxford, New York, pp.84-104.

[2] Raza J., Rohni A.M. and Omar Z. (2016): *Multiple solutions of mixed convective MHD Casson fluid flow in a channel*.– Journal of Applied Mathematics, vol.2016, pp.1-10, https://doi.org/10.1155/2016/7535793.

[3] Pramanik S. (2014): *Casson fluid flow and heat transfer past an exponential porous stretching surface in presence of thermal radiation*.– Ain Shams Eng. J., vol.5, No.1, pp.205-212, https://doi.org/10.1016/j.asej.2013.05.003.

[4] El-Aziz M.A. and Afify A.A. (2016): *Effects of variable thermal conductivity with thermal radiation on MHD flow and heat transfer of Casson liquid film over an unsteady stretching surface*.– Brazil. J. Phys., vol.46, pp.516-525, https://doi.org/10.1007/s13538-016-0442-3.

[5] Eldabe N.T.M. and Salwa M.G.E. (1995): *Heat transfer of MHD non-Newtonian Casson fluid flow between two rotating cylinders*.– J. Phys. Soc. Japan, vol.64, No.1, pp.41-64, https://doi.org/10.1143/JPSJ.64.41.

[6] Kishan N. and Shashidar B. (2013): *MHD effects on non-Newtonian power-law fluid past a continuously moving porous flat plate with heat flux and viscous dissipation*.– Int. J. Appl. Mech. Eng., vol.18, No.2, pp.425-446, https://doi.org/10.2478/ijame-2013-0026.

[7] Sadiq K., Siddique I., Khan I., Khan M.I. and Singh A. (2023): *Heat and mass transfer in a second grade nanofluids with wall slippage, heat generation and chemical reaction: exact solutions*.– Int. Commun. Heat Mass Tran., vol.148, pp.107024, https://doi.org/10.1016/j.icheatmasstransfer.2023.107024.

[8] Yanala D.R., Kumar M.A., Bejawada S.G., Nisar K.S., Raju R.S. and Rao V.S. (2023): *Exploration of heat and mass transfer on 3-D radiative MHD Casson fluid flow over a stretching permeable sheet with chemical reaction*.– Case Stud. Therm. Eng., vol.51, pp.103527, https://doi.org/10.1016/j.csite.2023.103527.

[9] Anwar M.S., Alqarni M.S. and Irfan M. (2024): *Exploring the marvels of heat transfer: MHD convection at a stagnation point in non-Newtonian fluid with yield stress and chemical reactions*.– Chin. J. Phys., vol.89, pp.1299-1308, https://doi.org/10.1016/j.cjph.2024.03.037.

[10] Shamshuddin M.D., Mabood F. and Salawu S.O. (2021): *Flow of three-dimensional radiative Williamson fluid over an inclined stretching sheet with Hall current and nth-order chemical reaction*.– Heat Transfer, vol.50, No.6, pp.5400-5417, https://doi.org/10.1002/htj.22130.

[11] Subbarayudu K., Suneetha S. and Bala Anki Reddy P. (2020): *The assessment of time dependent flow of Williamson fluid with radiative blood flow against a wedge*.– Propulsion and Power Research, vol.9, No.1, pp.87-99, https://doi.org/10.1016/j.jppr.2019.07.001.

[12] Makinde O.D. (2005): *Free convection flow with thermal radiation and mass transfer past a moving vertical porous plate*.– Int. Commun. Heat Mass Transf., vol.32, No.10, pp.1411-1419, https://doi.org/10.1016/j.icheatmasstransfer.2005.07.005.

[13] Das K. (2011): *Impact of thermal radiation on MHD slip flow over a flat plate with variable fluid properties*.– Heat Mass Transf., vol.48, No.5, pp.767-778, https://doi.org/10.1007/s00231-011-0927-4.

[14] Mukhtar T., Jamshed W., Aziz A. and Al-Kouz W. (2023): *Computational investigation of heat transfer in a flow subjected to magnetohydrodynamic of Maxwell nanofluid over a stretched flat sheet with thermal radiation*.– Numer. Methods Part. Differ. Equ., vol.39, No.5, pp.3499-3519, https://doi.org/10.1002/num.22643.

[15] Yacob N.A., Ishak A. and Pop I. (2011): *Melting heat transfer in boundary layer stagnation-point flow towards a stretching/shrinking sheet in a micropolar fluid*.– Comput. Fluids, vol.47, No.1, pp.16-21, https://doi.org/10.1016/j.compfluid.2011.01.040.

[16] Bachok N., Ishak A. and Pop I. (2010): *Melting heat transfer in boundary layer stagnation-point flow towards a stretching/shrinking sheet*.– Phys. Lett. A, vol.374, No.39, pp.4075-4079, https://doi.org/10.1016/j.physleta.2010.08.014.

[17] Mabood F. and Das K. (2016): *Melting heat transfer on hydromagnetic flow of a nanofluid over a stretching sheet with radiation and second-order slip*.– Eur. Phys. J. Plus, vol.131, No.3, pp.1-13, https://doi.org/10.1140/epjp/i2016-16056-1.

[18] Fazle M. and Kalidas D. (2019): *Outlining the impact of melting on MHD Casson fluid flow past a stretching sheet in a porous medium with radiation*.– Heliyon, vol.5, No.2, pp.e01216, https://doi.org/10.1016/j.heliyon.2019.e01216.

[19] Alsulami M.D. and Hymavathi D. (2023): *Melting heat transfer of micropolar nano fluid flow through porous medium*.– International Journal of Modern Physics B, vol.37, No.25, pp.2350294, https://doi.org/10.1142/S021797922350294X.

[20] Ehsan G., Bijarchi M., Kazemzadeh Hannani S. and Nouri-Boroujerdi A. (2024): *Evaluating Joule heating's influence on heat transfer and entropy generation in MHD channel flow: a parametric study and ill-posed problem solution using PINNs*.– arXiv, https://doi.org/10.48550/arXiv.2406.15810.

[21] Yuvaraju N., Hymavathi D., Ramesh K. and Shashidar Reddy B. (2024): *Joint effect of velocity slip and Joule heating MHD Casson-Williamson nanofluid passes through the stretching porous medium*.– Journal of Advanced Research in Fluid Mechanics and Thermal Sciences, vol.123, No.1, pp.156-171, https://doi.org/10.37934/arfmts.123.1.156171.

[22] Ahmad S., Khan M.N., Nadeem S., Rehman A., Ahmad H. and Ali R. (2021): *Impact of Joule heating and multiple slips on a Maxwell nanofluid flow past a slandering surface*.– Commun. Theor. Phys., vol.74, No.1, pp.015001, https://doi.org/10.1088/1572-9494/ac357d.

[23] Ramesh K., Hari Singh Naik, Shashidar Reddy B. and Christophe Ch. (2022): *Role of nanoparticles and heat source/sink on MHD flow of Cu-H2O nanofluid flow past a verticle plate with Soret and Dufour effects*.– Mathematical and Computational Applications, vol.27, No.6, pp.1-18, https://doi.org/10.3390/mca27060102.

[24] Narsimha Reddy B., Maddileti P. and Shashidar Reddy B. (2022): *Nanofluid flow on non-linearly stretching surface influenced by the combined effects of Soret and Dufour with chemical reaction*.– JP Journal of Heat and Mass Transfer, vol.30, pp.161-182, https://doi.org/10.17654/0973576322055.

[25] Rosseland S. (1931): *Astrophysik und Atom-theoretische Grundlagen*.– Springer-Verlag, Berlin.

[26] Shashidar Reddy B., Saritha K. and Venkata Madhu J. (2021): *Impact of chemical reaction on mass transfer and melting heat transfer of porous MHD Casson fluid flow*.– J. Math. Comput. Sci., vol.11, No.1, pp.149-164, https://doi.org/10.28919/jmcs/5086.

Received: August 01, 2025
Revised: February 16, 2026